ELSEVIER

Biochimica et Biophysica Acta 1416 (1999) 69–91

BIOCHIMICA ET BIOPHYSICA ACTA
BBA

Two-component blocking kinetics of open NMDA channels by organic cations

Alexander I. Sobolevsky *

Institute of General Pathology and Pathophysiology, Baltiyskaya 8, 125315 Moscow, Russia

Received 20 July 1998; received in revised form 27 October 1998; accepted 30 October 1998

Abstract

NMDA receptor channel responses were recorded from acutely isolated rat hippocampal neurons, using whole-cell patch-clamp techniques. In the continuous presence of aspartate, tetraethylammonium, tetrabutylammonium, 1-amino-3-propyl-adamantane and 9-aminoacridine caused changes in the current through NMDA channels, which were described by two-exponential functions. It was established that depending on the behavior of the amplitude of the fast component for the recovery kinetics, the blocker action can be assigned to one of five types described by the simplest models. The effects of tetraethylammonium, tetrabutylammonium and 1-amino-3-propyl-adamantane were well described by these models. Using 9-aminoacridine as an example, it was shown that the simplest models cannot describe all possible types of the blocker-channel interaction. In such cases, the method of the simplest models combination can be used. The application of the simplest kinetic models analysis allowed to make the following conclusions: at least two molecules of 1-amino-3-propyl-adamantane or 9-aminoacridine can simultaneously bind to the open channel and block it; the occupation of 9-aminoacridine blocking sites in the channel can proceed in at least two different ways; the binding of tetrabutylammonium and 9-aminoacridine prevented the closure of the activation and/or desensitization gates of the channel, while that of tetraethylammonium did not.

Keywords: *N*-Methyl-D-aspartate channel; Hippocampal neuron; Patch clamp; Kinetics; Blockade

1. Introduction

The two-component kinetics of *N*-methyl-D-aspartate (NMDA)-mediated current changes induced by different blockers were described earlier. Thus, in the continuous presence of the NMDA channel agonists the existence of two kinetic components was shown for memantine [1–3] and other aminoadamantanes [4], long-chain adamantanes [5,6]; tetraalkylammonium compounds [7,8]; 1,2,3,4-tetrahydro-9-aminoacridine and 9-aminoacridine [9,8]. As NMDA channels play an important role in the processes of learning and memory, it is important to gain insight into the origin of multi-component kinetics manifested by NMDA channel blockers, especially when it is considered that some of them can be used as drugs in the treatment of a wide variety of neurodegenerative diseases [10].

The present study provides a simple method of a two-component kinetic analysis of changes induced in the stationary NMDA-mediated current by the blocker application. The analysis consists in the consideration of the amplitude of the fast component for the kinetics of recovery from the blockade (A_{fast}) depending on the blocker concentration. The study

* Fax: +7-095-151-0421; E-mail: rans@rans.msk.ru

0005-2736/99/$ – see front matter
PII: S0005-2736(98)00211-9

of the A_{fast}-dependence on the blocker concentration allows one to describe the blocker action by one of the five simplest kinetic models or by their combination. The NMDA channel blockers: tetraethylammonium (TEA), tetrabutylammonium (TBA), 1-amino-3-propyl-adamantane or MRZ 2/178 (MRZ) and 9-aminoacridine (9-AA) were analyzed according to the A_{fast}-criterion. The kinetic models obtained for these blockers have made it possible to make conclusions about the number of blocking sites and the ways, by which the blockers reached these sites as well as about the blocker interaction with the gating machinery of the NMDA channel.

2. Materials and methods

Pyramidal neurons were acutely isolated from the CA1 region of rat hippocampus using 'vibrodissociation techniques' [11]. The experiments were begun not earlier than after 3 h incubation of the hippocampal slices in a solution containing (mM): NaCl, 124; KCl, 3; $CaCl_2$, 1.4; $MgCl_2$, 2; glucose, 10; $NaHCO_3$, 26. The solution was bubbled with carbogen at 32°C. During the whole period of isolation and current recording, nerve cells were washed with a Mg^{2+}-free solution (mM): NaCl, 140; KCl, 5; $CaCl_2$, 2; glucose, 15; Hepes, 10; pH 7.3. Fast replacement of the superfusion solutions was achieved by using the concentration-jump technique [11,12]. The currents were recorded at 18°C in the whole-cell configuration using micropipettes made from pyrex tubes and filled with an 'intracellular' solution (mM): CsF, 140; NaCl, 4; Hepes, 10; pH 7.2. Electric resistance of the filled micropipettes was 3–7 MΩ. Analog current signals were digitized at 1 kHz frequency.

Statistical analysis was performed using the scientific and technical graphics computer program Microcal Origin (version 3.5 for Windows). The data presented are mean ± S.D. except as noted; comparison of means was done by ANOVA, with $P < 0.05$ taken as significant.

The kinetic models used to simulate the blockers action were based on the conventional rate theory and used independent forward and reverse rate constants to simultaneously solve first-order differential equations representing the transitions between all possible states of the channel. The rate constants were calculated by the method described in Appendix A with the help of Mathcad (version 5.0). Differential equations were solved numerically using the algorithm analogous to that described previously [13].

MRZ 2/178 was synthesized by MERZ (Eckenheimer, Frankfurt-am-Main, Germany); tetraethylammonium and tetrabutylammonium were purchased from Aldrich (USA); 9-aminoacridine from Sigma (USA). The three-dimensional structures of these compounds were obtained with the help of the Molecular Modeling System HyperChem (Release 3 for Windows).

3. Results

Application of aspartate (ASP) in the saturating concentration of 100 μM at the membrane potential of −100 mV in a Mg^{2+}-free, 3 μM glycine-containing solution elicited an inward current through NMDA channels. After the initial fast rise ($\tau < 30$ ms) this current decreased down to the value, I_0, with the time constant varying from 250 to 750 ms. Such a current decay in the continuous presence of the agonist is a result of desensitization of the receptor–channel complex. Only after the current reached its stationary level, I_S, various NMDA channel blockers were applied in the continuous presence of ASP.

Magnesium (1 mM) caused a practically complete blockade of the ASP-induced current. The onset and the offset kinetics of Mg^{2+} were well fitted with single exponential functions (Fig. 1). The onset and offset time constants were: $\tau_{ON} = 9.24 \pm 2.84$ ms and $\tau_{OFF} = 137 \pm 71$ ms ($n = 11$), respectively. If these constants were defined by the association and dissociation of the blocker molecules, the mechanism of Mg^{2+} action can be described by the following simplest model:

$$O^* \underset{k_2}{\overset{k_1[B]}{\rightleftharpoons}} O_B$$

Model 1

where O and O_B represent the channel in the open and the open blocked states, respectively. The aster-

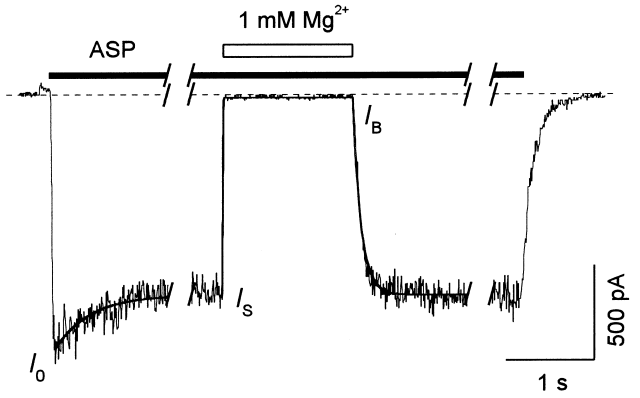

Fig. 1. The kinetics of Mg^{2+}-induced changes in the NMDA-mediated current. The current elicited by ASP (100 μM) gained its stationary level (I_S) decreasing from the maximal value (I_0) with the time constant of 482 ms (the fitting is shown by a solid line). Mg^{2+} (1 mM) was applied 20 s after the beginning of ASP application and induced a practically complete inhibition of the current. The time constant of the current decrease, $\tau_{ON} = 4.8$ ms. After the termination of Mg^{2+} application the current recovered with the time constant, $\tau_{OFF} = 112$ ms.

isk indicates the conducting state; k_1 and k_2 are the kinetic constants. [B] is the blocker concentration. As the experiments were carried out in the continuous presence of high concentrations of ASP and glycine; here and further it is suggested that all the agonist and co-agonist sites are completely occupied and, correspondingly, all the states of the channel represented in the models are the agonist and the coagonist bound ones. The association (k_1) and dissociation (k_2) constants for model 1 are defined from the following equations:

$$\tau_{ON} = 1/(k_1[B] + k_2) \quad (1)$$

and

$$\tau_{OFF} = 1/k_2 \quad (2)$$

The values of the association and dissociation rate constants defined from Eqs. 1 and 2 were the following: $k_1 = 1.01 \pm 0.36 \times 10^5$ $M^{-1}\,s^{-1}$ and $k_2 = 7.3 \pm 1.1$ s^{-1}. These values were much smaller than those defined in single-channel recording experiments [14]: $k_1 = 2.2 \times 10^8$ $M^{-1}\,s^{-1}$ and $k_2 = 640$ s^{-1}. Therefore, the association and dissociation kinetics of Mg^{2+} are really much faster than those predicted by our measurements and the time constants of the current increase at the beginning, τ_{ON}, and the current decrease at the end of Mg^{2+} application, τ_{OFF}, depend crucially on the onset and offset rates of the solution exchange system, respectively.

Many well-known blockers manifest multicomponent blocking kinetics of liganded NMDA channels. The changes in the ASP-induced current in response to the beginning and termination of TEA (5 mM), TBA (2 mM), 9-AA (40 μM) and MRZ (150 μM) applications after the plateau current had reached its stationary level (I_S) were fitted with the sum of the two exponents (Fig. 2A,B,C,D, respectively). The recovery kinetics will be studied in order to elucidate the mechanisms of the blockers action. These kinetics are easier to analyze than the blocking kinetics due to the conjectural independence of the recovery time constants on the blocker concentration. The current recovery after termination of the blocker action was fitted by the following equation (Fig. 2E):

$$I(t) = I_S + (I_B - I_S) \times \{A_{fast} \times \exp(-t/\tau_{fast}) + (1 - A_{fast}) \times \exp(-t/\tau_{slow})\} \quad (3)$$

where A_{fast} is the amplitude of the fast component, τ_{fast} and τ_{slow} are the fast and the slow time constants, respectively. The values of the parameters proved to be as follows: $A_{fast} = 0.63 \pm 0.02$, $\tau_{fast} = 198 \pm 14$ ms, and $\tau_{slow} = 2.43 \pm 0.17$ s for TEA; $A_{fast} = 2.12 \pm 0.24$, $\tau_{fast} = 105 \pm 8$ ms, and $\tau_{slow} = 289 \pm 29$ ms for TBA; $A_{fast} = 1.83 \pm 0.07$, $\tau_{fast} = 727 \pm 24$ ms, and $\tau_{slow} = 1.54 \pm 0.53$ s for 9-AA; $A_{fast} = -0.36 \pm 0.07$, $\tau_{fast} = 1.35 \pm 0.28$ s, and $\tau_{slow} = 5.48 \pm 0.20$ s for MRZ. The slow changes in the unblocking kinetics do not probably result from the action of other ion exchangers/transporters because no such slow kinetics was observed on the recovery from the Mg^{2+} block. It is evident that the value of A_{fast} did not obviously lie between 0 and 1 (TEA) but can be greater than 1 (TBA and 9-AA) and lower than 0 (MRZ). The proximity of τ_{fast} for TEA and TBA and the time constant of the current recovery after termination of Mg^{2+} application ($\tau_{OFF} = 137 \pm 71$ ms) may imply that the fast component of their unblocking is masked by the rate of the solution replacement. This can explain the apparent inadequacy of the double exponential fit of the recovery kinetics in the case of TBA (Fig. 2E).

To elucidate the mechanism of the blocker action,

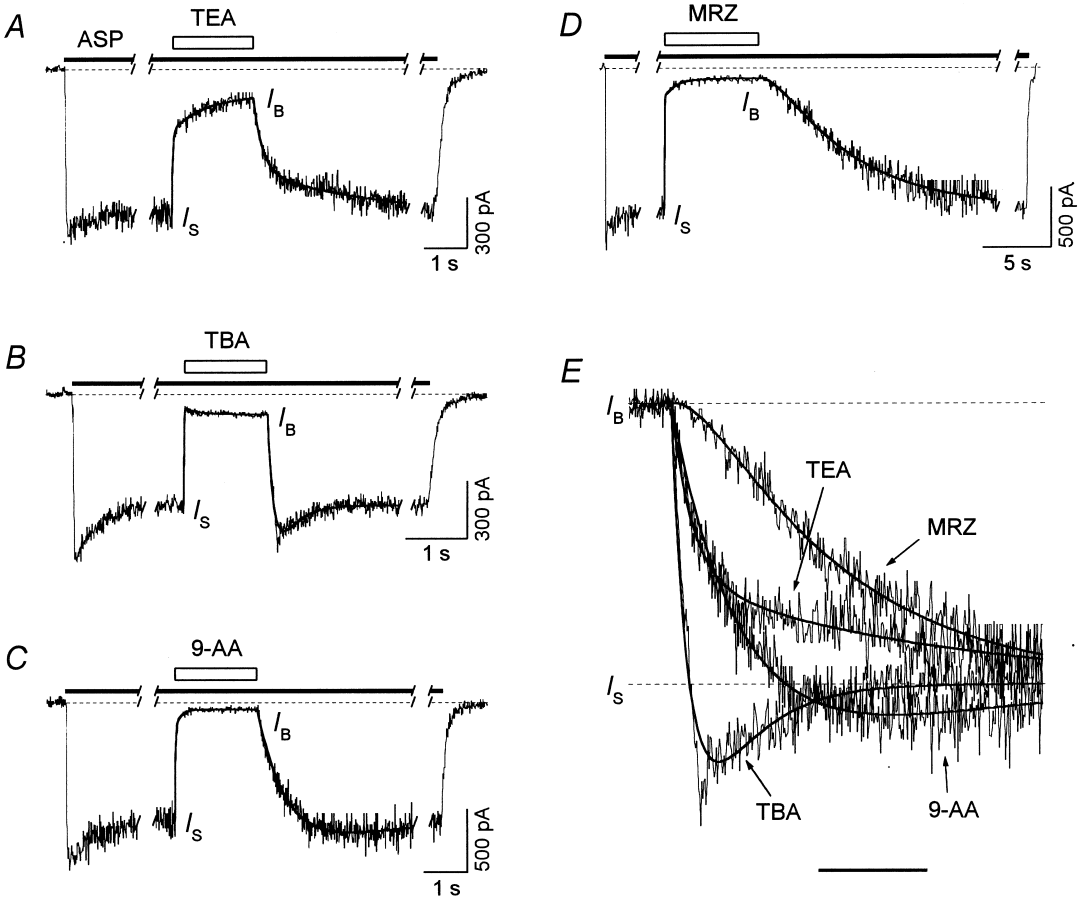

Fig. 2. The two-component kinetics of the NMDA channels blockade. The experimental protocol is the same as shown in Fig. 1. 5 mM TEA (A), 2 mM TBA (B), 40 μM 9-AA (C) and 150 μM MRZ (D) were applied against the background of ASP (100 μM). The current changes induced by the beginning and termination of the blocker application were fitted with double exponential functions (solid lines). (E) The recovery kinetics from A–D are presented on an expanded time scale. The fittings were made with Eq. 3 (solid lines). Note that the value of A_{fast} was equal to 0.63 for TEA, 2.12 for TBA, 1.83 for 9-AA and −0.36 for MRZ. The bar is equal to 1 s for TEA and 9-AA, 0.6 s for TBA and 4 s for MRZ.

all possible models with three states of the channel were considered. These models are the simplest which can simulate the two-component blocking kinetics. As in the previous study [4], the behavior of the amplitude of the fast component (A_{fast}) depending on the blocker concentration was taken as a criterion of discrimination between these models. There are only five simplest models with three states which describe the blocker and the channel interaction in the continuous presence of the saturating concentration of the agonist. Two of them are parallel. The first one is the following:

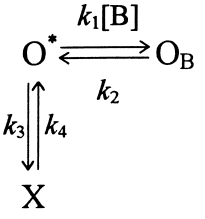

Model 2

where X can represent the closed (C) or the desensitized (D) state of the channel or their combination, which provides the kinetics with the rate-limiting

transitions from the open state with the constant, k_3, and to the open state with the constant, k_4. The amplitude of the fast component does not depend on the blocker concentration and, if $k_2 > k_3+k_4$, is defined by the following equation (see Appendix A):

$$A_{fast} = 1-\frac{k_2 \cdot k_3}{k_4 \cdot (k_3 + k_4 - k_2)} \quad (4)$$

In the case when $k_2 < k_3+k_4$, the amplitude of the fast component will be equal to $1-A_{fast}$, where A_{fast} is defined from Eq. 4. The second parallel model is:

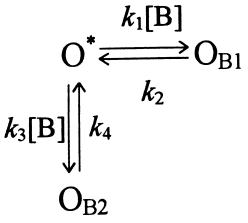

Model 3

where O_{B1} and O_{B2} represent the two open blocked states of the channel corresponding to two different blocker binding sites. The amplitude of the fast component does not depend on the blocker concentration and, if $k_2 > k_4$, is defined by the following equation (see Appendix A):

$$A_{fast} = \frac{1}{1+\frac{k_2 \cdot k_3}{k_1 \cdot k_4}} \quad (5)$$

The values of A_{fast} defined by Eq. 5 are within the interval between 0 and 1. There are three sequential kinetic models. The first one is as follows:

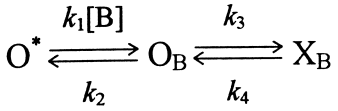

Model 4

where X_B may represent other open (O_{B2}) or closed (C_B) or desensitized (D_B) blocked states of the channel. The amplitude of the fast component does not depend on the blocker concentration and, if $k_2+k_3 > k_4$, is defined by the following equation (see Appendix A):

$$A_{fast} = \frac{1}{1-\frac{\lambda_1^2 \cdot (k_4+\lambda_2)}{\lambda_2^2 \cdot (k_4+\lambda_1)}} \quad (6)$$

where

$$\lambda_{1,2} = -0.5 \cdot \{(k_2+k_3+k_4) \pm [(k_2+k_3+k_4)^2 - 4 \cdot k_2 \cdot k_4]^{0.5}\}.$$

In the case when $k_2+k_3 < k_4$, the amplitude of the fast component will be equal to $1-A_{fast}$, where A_{fast} is defined from Eq. 6. It is easy to demonstrate that the values of A_{fast} defined by Eq. 6 lie within the interval between 0 and 1. The second sequential kinetic model is as follows:

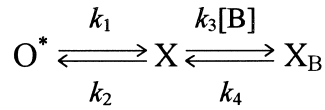

Model 5

where X can represent the closed (C) or the desensitized (D) and X_B, the closed blocked (C_B) or the desensitized blocked (D_B) states of the channel, respectively. The amplitude of the fast component does not depend on the blocker concentration either and, when $k_1+k_2 > k_4$, is defined by the following equation (see Appendix A):

$$A_{fast} = \frac{k_4}{k_4 - k_1 - k_2} \quad (7)$$

In the case when $k_1+k_2 < k_4$, the amplitude of the fast component will be equal to $1-A_{fast}$, where A_{fast} is defined from Eq. 7. In both cases, however, the value of the amplitude of the fast component is negative (and equal to zero when $k_1+k_2 = k_4$). Finally, the third sequential model is as follows:

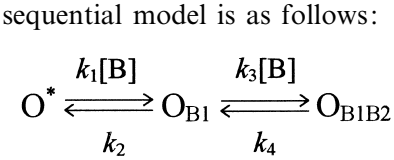

Model 6

where O_{B1B2} represents the open blocked state, in which two blocker molecules simultaneously bind to the channel. The amplitude of the fast component decreases with the blocker concentration and, when $k_2 > k_4$, is defined by the following equation (see Appendix A):

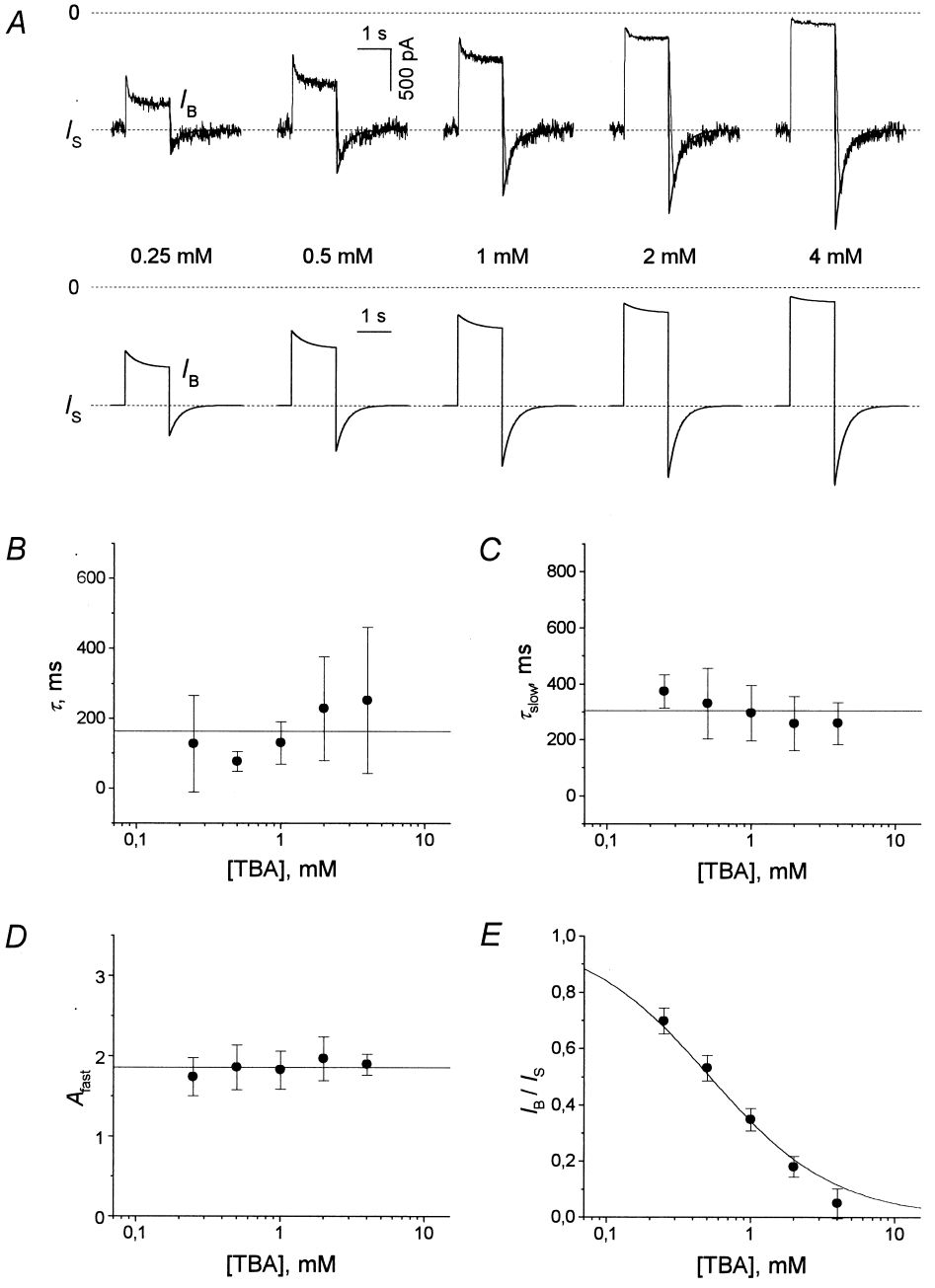

Fig. 3. The kinetics of TBA. (A) The experimental (first row) and modeling (second row) current traces in response to the application of different concentrations of TBA (0.25–4 mM) in the continuous presence of ASP (100 μM). The recovery kinetics of the experimental currents were fitted with Eq. 3 at fixed $\tau_{fast} = 1$ ms (solid lines). (B) The time constant, τ, obtained by the monoexponential fitting of the fast descending phase of the current recovery after termination of TBA application. τ was essentially independent of the blocker concentration and was equal, on average, to 163 ± 142 ms, $n = 7$ (horizontal line). (C,D) The slow time constant and the amplitude of the fast component obtained by the fitting of the current recovery after termination of TBA application with Eq. 3 at fixed $\tau_{fast} =$ 1 ms. Their values were essentially independent of TBA concentration and were, on average, $\tau_{slow} = 304 \pm 99$ ms and $A_{fast} = 1.86 \pm 0.24$, $n = 7$ (horizontal lines). (E) The concentration dependence of the stationary block (I_B/I_S) which was fitted with Eq. A9 (solid line). The value of the parameter K is equal to $1.91 \pm 0.18 \times 10^3$ M^{-1}, $n = 7$.

$$A_{fast} = \frac{1-\frac{k_3}{k_2-k_4}[B]}{1+\frac{k_3}{k_4}[B]} \quad (8)$$

In the case when $k_2 < k_4$, the amplitude of the fast component will be equal to $1-A_{fast}$ where A_{fast} is defined from Eq. 8. Eq. 8 predicts that A_{fast} becomes negative at the values of the blocker concentration, [B], greater than $(k_2-k_4)/k_3$.

3.1. The kinetics of TBA

Fig. 3A (first row) gives an example of application of different concentrations of TBA (0.25–4 mM) in the continuous presence of ASP (100 μM). The fitting of the descending phase of the current response to the termination of TBA application by the single exponential function yielded the fast time constant, τ, which was essentially independent ($P > 0.05$) of TBA concentration (Fig. 3B). The mean value of τ proved to be 163 ± 142 ms ($n = 7$) and was not significantly different from the time constant of the current recovery after termination of Mg^{2+} application ($\tau_{OFF} = 137 \pm 71$ ms). Thus, one may suppose that the real fast component of the channels recovery from the TBA block is very fast and is masked by the process of the solution exchange. Indeed, in the study of the interaction of TBA with the gating machinery of NMDA channels using the kinetic models [8], the value of the fast time constant of TBA unblocking was 1000 s^{-1} stipulating the fast time constant, $\tau_{fast} = 1$ ms. Thus, it is clear that the fitting shown in Fig. 2E for TBA is inadequate. The fitting of the current recovery by Eq. 3 after termination of TBA application was carried out with fixed $\tau_{fast} = 1$ ms in the interval excluding the fast current decrease, which reflected the process of solution exchange (Fig. 3A, first row, solid lines). The value of τ_{fast} was taken to be low enough and its decrease did not lead to the variations in other parameters (τ_{slow} and A_{fast}) of Eq. 3. In Fig. 3C,D, respectively, the values of τ_{slow} and A_{fast} are plotted as a function of TBA concentration. Neither of these parameters depended on the blocker concentration ($P > 0.05$); their mean values were as follows: $\tau_{slow} = 304 \pm 99$ ms and $A_{fast} = 1.86 \pm 0.24$ ($n = 7$).

It is important to emphasize that fixation of the parameter τ_{fast} did not affect the behavior of the parameters τ_{slow} and A_{fast} depending on TBA concentration. Thus, the fitting of TBA recovery kinetics with non-fixed τ_{fast} (see Fig. 2E) gave the same result: neither τ_{slow} nor A_{fast} depended on the blocker concentration ($P > 0.05$), although the mean value of τ_{slow} (273 ± 94 ms) was slightly lower and the mean value of A_{fast} (2.29 ± 0.62) was slightly higher than the corresponding values obtained with $\tau_{fast} = 1$ ms. The cases when $\tau_{fast} = 1$ ms and with non-fixed τ_{fast} limited the range of τ_{fast} values, which affected τ_{slow} and A_{fast} (in the case of $\tau_{fast} < 1$ ms the values of τ_{slow} and A_{fast} were practically the same as in the case of $\tau_{fast} = 1$ ms, i.e., the value $\tau_{fast} = 1$ ms can be considered as minimal; in the case of non-fixed τ_{fast} the value of τ_{fast} was maximal). At any value of this range τ_{slow} and A_{fast} (> 1) did not vary with the blocker concentration.

Therefore, the arbitrary choice of the value of τ_{fast} for fitting did not affect the choice of the kinetic model because as the value of A_{fast} did not depend on the blocker concentration and was greater than unity, the only simplest model which can describe the kinetics of the TBA action is model 2. The degree of the stationary blockade predicted by this model is defined by Eq. A9 (see Appendix A). The value of the parameter K for this equation was equal to $1.91 \pm 0.18 \times 10^3$ M^{-1}, $n = 7$ (Fig. 3E). The system of equations which was obtained by the substitution of the mean values of the parameters τ_{slow}, A_{fast} and

Table 1
The kinetic constants for TEA, TBA and MRZ

Compound	Model	k_1, 10^6 M^{-1} s^{-1}	k_2, s^{-1}	k_3	k_4, s^{-1}
TBA	2	3.5	10^3	1.52 s^{-1}	1.77
TEA	3	0.523	10^3	118 M^{-1} s^{-1}	0.47
	4	0.516	10^3	0.24 s^{-1}	0.47
MRZ	6	0.088	1.14	1.4×10^4 M^{-1} s^{-1}	0.13

K, and $\tau_{fast} = 1$ ms into Eq. A4, Eq. A5, Eq. 4 and Eq. A9 made it possible to estimate the values of all kinetic constants. The values of k_1, k_2, k_3 and k_4 for TBA are presented in Table 1. Fig. 3A (second row) shows the currents predicted by model 2 at these values of the kinetic constants.

As the choice of the kinetic model describing TBA action depended on the behavior of the fitting parameters τ_{slow} and A_{fast}, it is important to establish the effect of the solution exchange time, τ_{wash}, on the values of these parameters (assuming that the solution exchange is a single-exponential process, [13]). Fig. 4A shows the recovery of the currents predicted by model 2 at different values of τ_{wash}. The typical example of the experimental current recovery is shown in Fig. 4B. This curve was fitted with Eq. 3 as was described above (Fig. 4B, thin smooth line). In this case the solution exchange is instantaneous. If we compare Fig. 4A and B, it becomes clear that always at τ_{wash} values of the range of τ_{fast} value (1 ms) the recovery looks like those when the solution exchange is instantaneous. In reality, τ_{wash} is much greater than τ_{fast}. This is why the real experimental curve is better approximated by the modeling curve with $\tau_{wash} = 30$ ms (Fig. 4B, thick smooth line). The modeling curves at $\tau_{wash} = 1$, 30 and 100 ms and different blocker concentrations were fitted in the same way as the experimental curves (with $\tau_{fast} = 1$ ms). The values of the parameters τ_{slow} and A_{fast} depending on the blocker concentration are shown in Fig. 4C,D, respectively. It can be seen that τ_{slow} rose with an increase in τ_{wash} remaining practically concentration-independent. An essential increase in A_{fast} with concentration was observed only at high values of

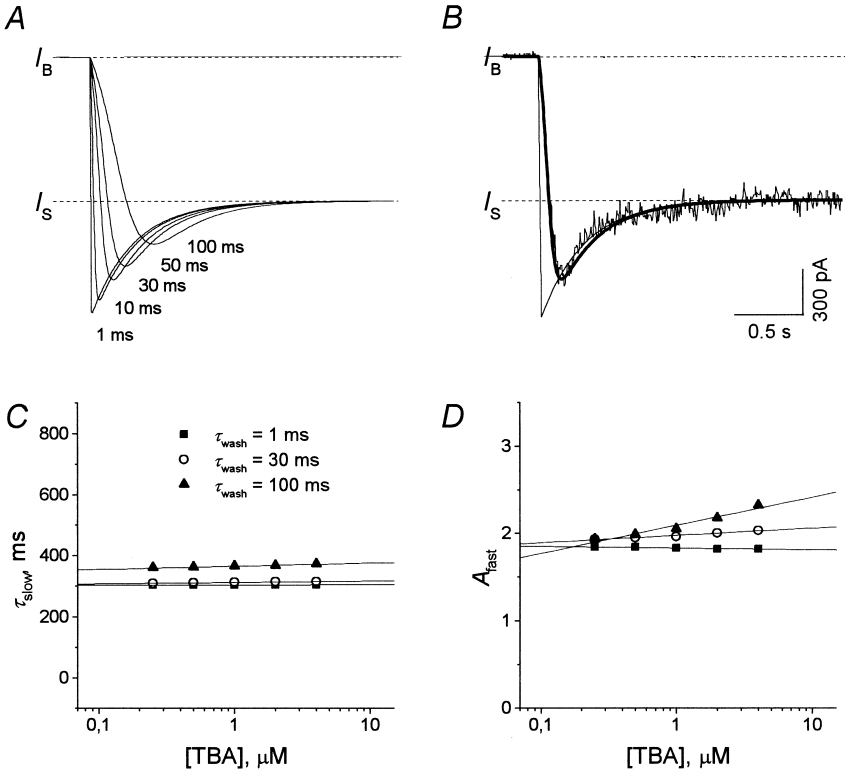

Fig. 4. The dependence of the recovery kinetics predicted by model 2 for TBA on the solution exchange time. (A) The current recovery predicted by model 2 at different values of the solution exchange time, τ_{wash} (1, 10, 30, 50, and 100 ms). TBA concentration is 2 mM. (B) An example of an experimental current recovery. TBA concentration is 2 mM. The thin smooth line shows the fitting of the current with Eq. 3 at fixed $\tau_{fast} = 1$ ms. The thick smooth line is the normalized modeling current at $\tau_{wash} = 30$ ms. (C,D) The slow time constant and the amplitude of the fast component obtained by the fitting of the modeling current recovery with Eq. 3 at fixed $\tau_{fast} = 1$ ms at different values of τ_{wash} (1, 30, and 100 ms) depending on the blocker concentration. Solid lines show the apparent linear fit.

τ_{wash} (100 ms). In experiments with TBA the mean value of τ_{wash} was approximately 30 ms (the corresponding value of $\tau = 163$ ms). At this value of τ_{wash} the parameters τ_{slow} and A_{fast} did not practically depend on the blocker concentration (open circles in Fig. 4C,D) and the small vertical shift of the τ_{slow} and A_{fast} concentration dependencies was smaller than the value of the experimental error (cf. Fig. 4C with Fig. 3C and Fig. 4D with Fig. 3D). Therefore, the non-instantaneous solution exchange did not significantly affect the values and behavior of the fitting parameters and, correspondingly, did not affect the choice of the simplest model, which describes the kinetics of TBA action. Possible minor changes in the values of the kinetic constants due to the non-instantaneous solution exchange are not a matter of principle.

3.2. The kinetics of TEA

Fig. 5A (first row) shows an example of application of different concentrations of TEA (0.625–10 mM) in the continuous presence of ASP (100 μM). The fitting of the recovery kinetics with Eq. 3 by analogy with the fitting presented in Fig. 2E yielded the value of the fast time constant, which was essentially independent ($P > 0.05$) of TEA concentration (Fig. 5B). The mean value of τ_{fast} proved to be 218 ± 52 ms ($n = 4$) and was not significantly different from the time constant of the current recovery after termination of Mg^{2+} application ($\tau_{OFF} = 137 \pm 71$ ms). This finding prompts an idea that, as in the case of TBA, the fast component of the channels recovery from the TEA block is masked by the process of the solution exchange. Indeed, in the single-channel study [15], the dissociation of TEA from the NMDA channel was considered to be too fast to be measured at the sampling frequency of 4 kHz. Thus, the value of τ_{fast} should be less than 1 ms. It is clear that the fitting shown in Fig. 2E for TEA is inadequate. The fitting by Eq. 3 of the current recovery after termination of TEA application was carried out with fixed $\tau_{fast} = 1$ ms in the interval excluding the fast current decrease reflected the process of the solution exchange (Fig. 5A, first row, solid lines). The value of τ_{fast} was taken small enough and its decrease caused no variations in other parameters (τ_{slow} and A_{fast}) of Eq. 3. The values of τ_{slow} and A_{fast} as a function of TEA concentration are presented in Fig. 5C and D, respectively. None of these parameters depended on the blocker concentration ($P > 0.05$) and their mean values proved to be as follows: $\tau_{slow} = 2.14 \pm 0.61$ s and $A_{fast} = 0.67 \pm 0.09$ ($n = 4$).

As in the case of TBA, fixation of the parameter τ_{fast} did not affect the behavior of the parameters τ_{slow} and A_{fast} depending on TEA concentration. The fitting of TEA recovery kinetics with non-fixed τ_{fast} (see Fig. 2E) gave the same result: neither τ_{slow}, nor A_{fast} depended on the blocker concentration ($P > 0.05$), although the mean values of τ_{slow} (2.75 ± 0.88 s) and A_{fast} (0.72 ± 0.03) were slightly higher than the corresponding values obtained with $\tau_{fast} = 1$ ms. Therefore, as in the case of TBA, the arbitrary choice of the value of τ_{fast} for fitting will not affect the choice of the kinetic models describing the TEA action.

As the value of A_{fast} did not depend on the blocker concentration and was greater than 0, the three simplest models which can describe the kinetics of TEA action are models 2, 3 and 4. The degree of the stationary blockade predicted by these models is defined by Eq. A9 (see Appendix A). The value of the parameter K for this equation was equal to 777 ± 82 M^{-1}, $n = 4$ (Fig. 5E). The systems of equations obtained by the substitution of the mean values of the parameters τ_{slow}, A_{fast}, and K and $\tau_{fast} = 1$ ms into Eq. A4, Eq. A5, Eq. 4 and Eq. A9 for model 2, Eq. A4, Eq. A5, Eq. 5 and Eq. A9 for model 3 and Eq. A4, Eq. A5, Eq. 6 and Eq. A9 for model 4 allowed to estimate the values of the kinetic constants. The values of the kinetic constants for model 2 proved to be the following: $k_1 = 0.52 \times 10^6$ M^{-1} s^{-1}; $k_2 = 0.47$ s^{-1}; $k_3 = 999$ s^{-1} and $k_4 = 0.69$ s^{-1}. The state X cannot be the desensitized state in this case because the value of k_3 is three order of magnitude smaller than the kinetic constant of the transition from the open to the desensitized state [16]. Alternatively, if state X is the closed state, then the open probability, P_0 is equal to $k_4/(k_3+k_4) < 10^{-3}$. However, the value of P_0 for NMDA channels was found to vary from 0.04 to 0.5 [16–21]. Therefore, X in model 2 cannot be either the closed or desensitized state of the channel. Thus, model 2 cannot describe the real mechanism of the TEA interaction with NMDA channels.

The values of k_1, k_2, k_3 and k_4 for models 3 and 4

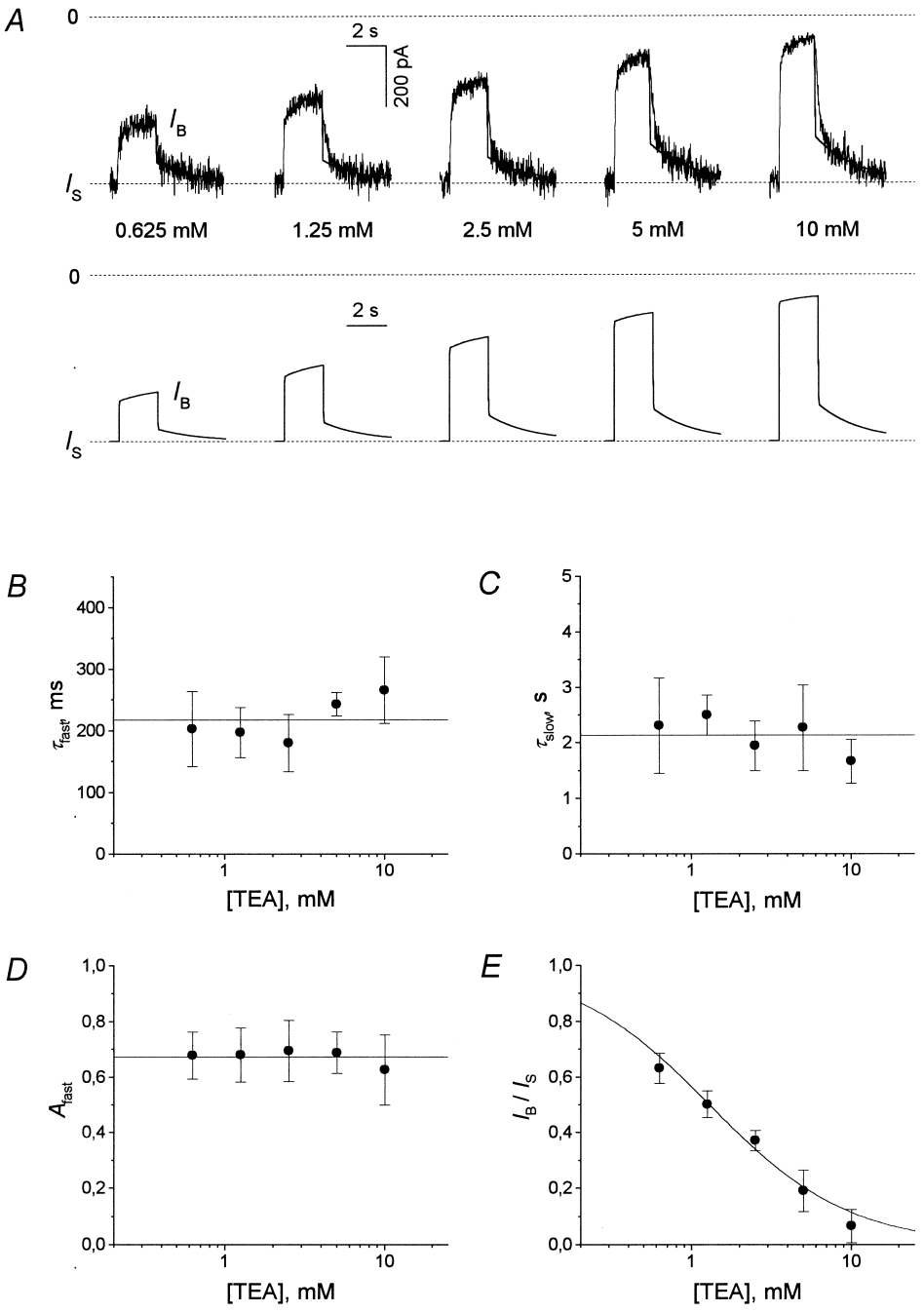

Fig. 5. The kinetics of TEA. (A) The experimental (first row) and modeling (second row) current traces in response to the application of different concentrations of TEA (0.625–10 mM) in the continuous presence of ASP (100 μM). The recovery kinetics of the experimental currents were fitted with Eq. 3 with fixed $\tau_{fast} = 1$ ms (solid lines). (B) The fast time constant obtained from the fitting of the current recovery after termination of TEA application with Eq. 3. τ_{fast} was essentially independent of the blocker concentration and was equal, on the average, to 218 ± 52 ms, $n = 4$ (horizontal line). (C,D) The slow time constant and the amplitude of the fast component obtained from the fitting of the current recovery after termination of TEA application with Eq. 3 at fixed $\tau_{fast} = 1$ ms. Their values were essentially independent of TEA concentration and were, on average, $\tau_{slow} = 2.14 \pm 0.61$ s and $A_{fast} = 0.67 \pm 0.09$, $n = 4$ (horizontal lines). (E) The concentration dependence of the stationary block (I_B/I_S), which was fitted with Eq. A9 (solid line). The value of the parameter K is equal to 777 ± 82 M^{-1}, $n = 4$.

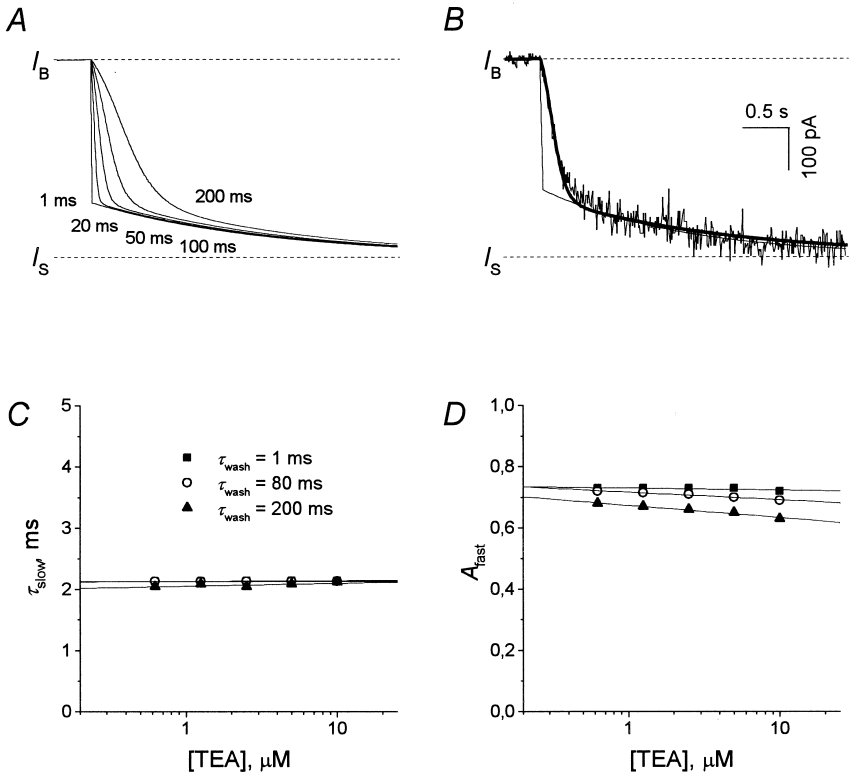

Fig. 6. The dependence of the recovery kinetics predicted by model 4 for TEA on the solution exchange time. (A) The current recovery predicted by model 4 at different values of the solution exchange time, τ_{wash} (1, 20, 50, 100, and 200 ms). TEA concentration is 10 mM. (B) An example of an experimental current recovery. TEA concentration is 10 mM. The thin smooth line shows the fitting of the current with Eq. 3 at fixed $\tau_{fast} = 1$ ms. The thick smooth line is the normalized modeling current at $\tau_{wash} = 80$ ms. (C,D) The slow time constant and the amplitude of the fast component obtained by the fitting of the modeling current recovery with Eq. 3 at fixed $\tau_{fast} = 1$ ms at different values of τ_{wash} (1, 80, and 200 ms) depending on the blocker concentration. The solid lines show the apparent linear fit.

are presented in Table 1. Fig. 5A (second row) shows the currents predicted by model 4. The currents predicted by model 3 are exactly the same.

The dependence of the recovery kinetics predicted by model 4 for TEA on the solution exchange time is shown in Fig. 6A. The typical experimental curve (Fig. 6B) was well approximated by modeling curve with $\tau_{wash} = 80$ ms (Fig. 6B, thick smooth line). The values of the parameters τ_{slow} and A_{fast} depending on the blocker concentration are shown in Fig. 6C,D, respectively. It can be seen that τ_{slow} did not practically depend on τ_{wash} and TEA concentration. An essential decrease in A_{fast} with concentration was observed only at high values of τ_{wash} (200 ms). In experiments with TEA the mean value of τ_{wash} was approximately equal to 80 ms (the corresponding value of τ_{fast} is 218 ms). At this value of τ_{wash}, the parameters τ_{slow} and A_{fast} did not practically depend on the blocker concentration (open circles in Fig. 6C,D) and the small vertical shift of the τ_{slow} and A_{fast} concentration dependencies was much smaller than the value of the experimental error (cf. Fig. 6C with Fig. 5C and Fig. 6D with Fig. 5D). The results for model 3 were quite the same. Therefore, the non-instantaneous solution exchange did not significantly affect the values and behavior of the fitting parameters and, correspondingly, did not affect the choice of the simplest model, which describes the kinetics of TEA action. As in the case of TBA, possible small changes in the values of the kinetic constants due to the non-instantaneous solution exchange are not a matter of principle.

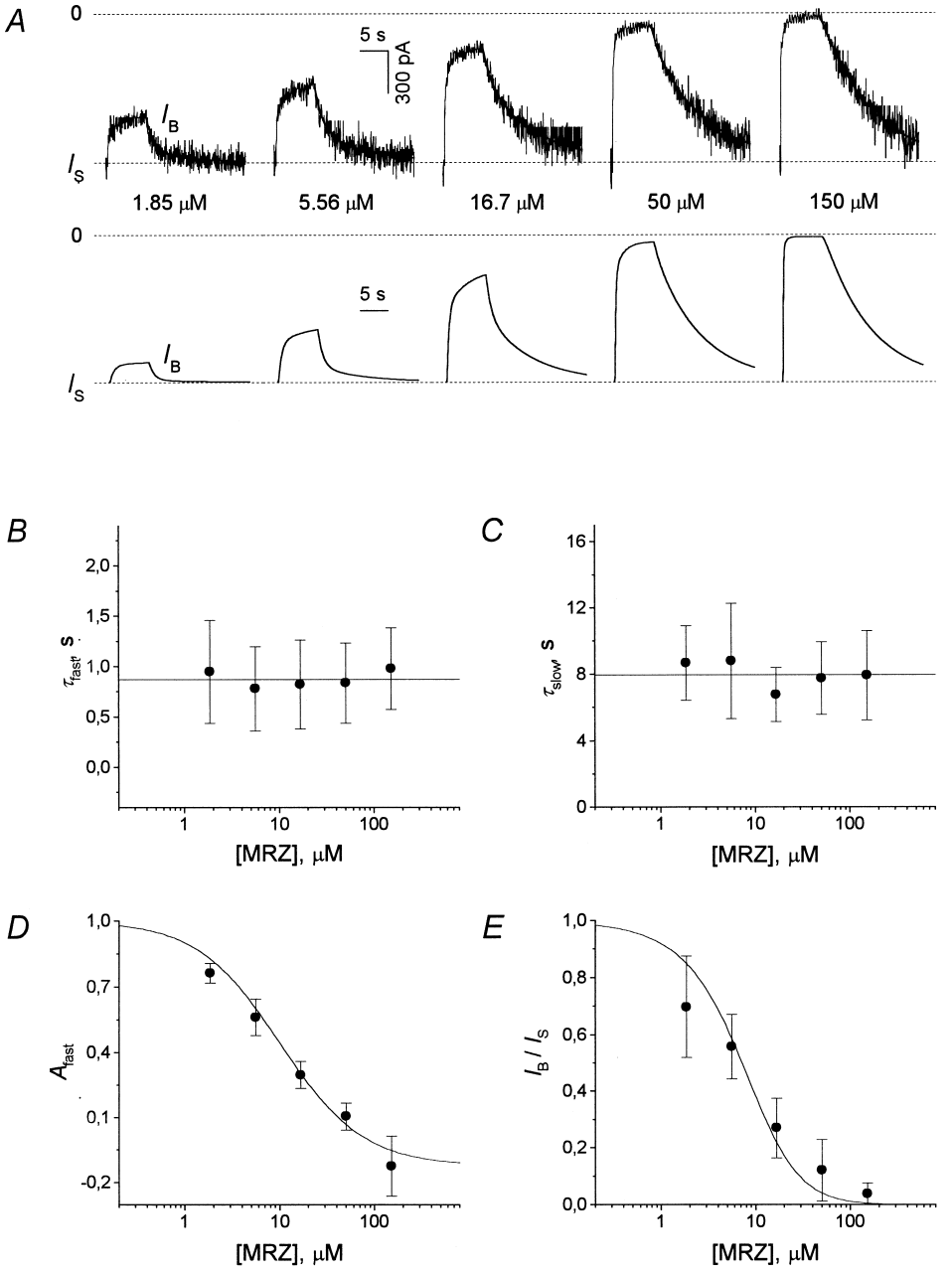

Fig. 7. The kinetics of MRZ. (A) The experimental (first row) and modeling (second row) current traces in response to application of different concentrations of MRZ (1.85–150 μM) in the continuous presence of ASP (100 μM). The recovery kinetics of the experimental currents were fitted with Eq. 3 (solid lines). (B–D) The fast and the slow time constants and the amplitude of the fast component of the current recovery. The values of τ_{fast} and τ_{slow} were essentially independent of MRZ concentration and were equal to 0.87 ± 0.41 s and 8.0 ± 2.6 s ($n = 12$), respectively (horizontal lines). A_{fast} decreased with MRZ concentration. The A_{fast} dependence on the blocker concentration was fitted with Eq. 8 at fixed $k_2 = 1.14$ s^{-1} and $k_4 = 0.13$ s^{-1} (solid line). The value of k_3 proved to be $1.4 \pm 0.2 \times 10^4$ $M^{-1}\,s^{-1}$ ($n = 12$). (E) The concentration dependence of the stationary block. I_B/I_S dependence on MRZ concentration was fitted with Eq. A10 (solid line). The value of the unknown parameter, k_1, proved to be of $8.8 \pm 3.2 \times 10^4$ $M^{-1}\,s^{-1}$ ($n = 12$).

3.3. The kinetics of MRZ

Fig. 7A (first row) gives an example of application of different concentrations of MRZ (1.85–150 μM) in the continuous presence of ASP (100 μM). The fitting of the recovery kinetics with Eq. 3 (solid lines) showed that neither the fast, nor the slow time constants depended ($P > 0.05$) on MRZ concentration (Fig. 7B,C). The mean values of τ_{fast} and τ_{slow} were 0.87 ± 0.41 s and 8.0 ± 2.6 s ($n = 12$), respectively. In contrast with tetraalkylammonium compounds, the amplitude of the fast component decreased with a rise in the blocker concentration (Fig. 7D). The values of A_{fast} at different concentrations were significantly different ($P < 0.05$). model 6 is the only simplest model predicted the changes in A_{fast} with the blocker concentration. The Eq. A4 and Eq. A5 of Appendix A for model 6 are as follows: $k_2 = 1/\tau_{fast}$ and $k_4 = 1/\tau_{slow}$. The values of the dissociation constants defined from them allowed to fit the A_{fast} dependence on MRZ concentration by Eq. 8 with only one unknown parameter, k_3 (Fig. 7D). The value of k_3 proved to be $1.4 \pm 0.2 \times 10^4$ $M^{-1} s^{-1}$. The approximated value of A_{fast} at infinitely high MRZ concentrations is equal to $-k_4/(k_2-k_4)$ and is negative (-0.123). The decrease in the fraction of the stationary block with a rise in MRZ concentration fitted by Eq. A10 with k_2, k_3 and k_4 equal to their mean values found above (Fig. 7E) allowed to estimate the value of $k_1 = 8.8 \pm 3.2 \times 10^4$ $M^{-1} s^{-1}$. It should be noted that the fitting of the concentration dependence of the stationary block with the logistic equation gave the values of the half-blocking concentration, $IC_{50} = 10.3 \pm 3.3$ μM and the Hill coefficient, $n_{Hill} = 1.34 \pm 0.26$ ($n = 12$). The high value of n_{Hill} supports the idea that not only one but two molecules of MRZ can bind to the NMDA channel. The values of all kinetic constants for MRZ are given in Table 1. The corresponding current traces predicted by model 6 are shown in Fig. 7A (second row). The inadequacy of model 6 for the description of the MRZ interaction with NMDA channels can be seen from the more steeper dependence of the stationary block fraction predicted by model 6 than that obtained in the experiment. Thus, the changes in the stationary current produced by the blocker application at low concentrations are considerably smaller for the model than for the experiment (cf. Fig. 7A, first and second rows). Correspondingly, the mean values of I_B/I_S at low MRZ concentrations lay below the fitting curve in Fig. 7E. This fact can be explained by the existence of a NMDA channel population with a high affinity for MRZ and, in contrast with model 6, by the existence of a non-strict succession, in which two blocking molecules can bind to their specific sites [4].

In contrast to TBA and TEA, the value of the fast time constant for MRZ was much higher than the value of the solution exchange time. Therefore in the case of MRZ the solution exchange was fast enough not to affect the definition of time and, correspondingly, kinetic constants.

3.4. The kinetics of 9-AA

Fig. 8A (first row) gives an example of application of different concentrations of 9-AA (2.5–40 μM) in the continuous presence of ASP (100 μM). The fitting of the recovery kinetics with Eq. 3 (solid lines) showed that the fast time constant increased exponentially with 9-AA concentration (Fig. 8B) - from 180 ± 56 ms (S.E., $n = 7$) at 2.5 μM up to the stationary level of 648 ± 56 ms (S.E., $n = 7$), the concentration constant being 6.8 ± 1.5 μM ($n = 7$). The values of τ_{fast} at different concentrations were significantly different ($P < 0.05$). The slow time constant was essentially independent ($P > 0.05$) of 9-AA concentration (Fig. 8C). The mean value of τ_{slow} proved to be 2.13 ± 1.11 s ($n = 7$). The amplitude of the fast component increased with a rise in the blocker concentration (Fig. 8D). The values of A_{fast} at different concentrations were significantly different ($P < 0.05$). The increase in the amplitude of the fast component with the blocker concentration is not predicted by any simplest models. What combination of the simplest models can simulate the experimentally observed 9-AA kinetics? Firstly, the resulting model should contain model 6, for which A_{fast} changes with the blocker concentration. Otherwise, any combination of models with A_{fast} independent on the blocker concentration will manifest the kinetics with the amplitudes of components that are also independent on the blocker concentration. model 6 is also the only simplest model, which suggests that not one but two blocker molecules can bind to the NMDA channel. This suggestion is supported by the steepness of the

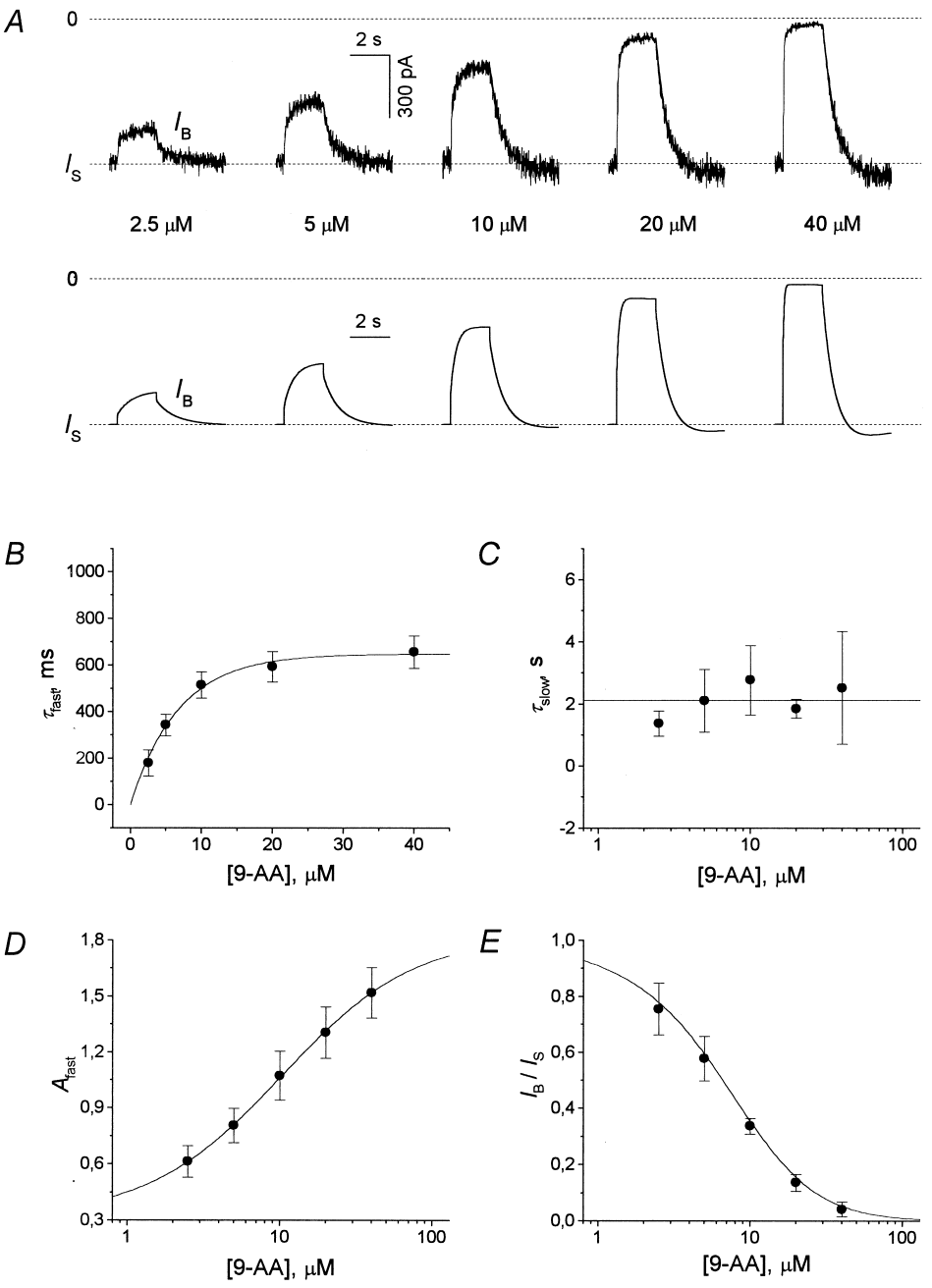

Fig. 8. The kinetics of 9-AA. (A) The experimental (first row) and modeling (second row) current traces in response to the application of different concentrations of 9-AA (2.5–40 μM) in the continuous presence of ASP (100 μM). The recovery kinetics of the experimental currents were fitted with Eq. 3 (solid lines). (B) The τ_{fast} (mean ± S.E.) dependence on 9-AA concentration. The fast time constant of the recovery increased exponentially with the concentration constant of 6.8 ± 1.5 μM, $n = 7$ (solid line). (C) The slow time constant of the current recovery. The value of τ_{slow} was essentially independent of 9-AA concentration and was equal, on the average, to 2.13 ± 1.11 s, $n = 7$ (horizontal line). (D) The amplitude of the fast component of the current recovery. A_{fast} increased with 9-AA concentration. The fitting of the A_{fast} dependence on the blocker concentration with Eq. 9 gave the following values of parameters: $a = 0.56 \pm 0.33$, $b = 3.14 \pm 1.00$ and $c = 0.30 \pm 0.20$ ($n = 7$). (E) The concentration dependence of the stationary block. The I_B/I_S dependence on the 9-AA concentration was fitted with Eq. A13 (solid line). The values of parameters are as follows: $a = 0.091 \pm 0.045$ and $b = 0.0109 \pm 0.0045$ ($n = 7$).

9-AA dose–response relationship shown in Fig. 8E. Thus, the fitting of the I_B/I_S dependence with the logistic equation gave the value of $IC_{50} = 6.3 \pm 0.6$ μM and a high value of $n_{Hill} = 1.56 \pm 0.20$ ($n = 7$). Secondly, the experimentally observed dependence of A_{fast} on 9-AA concentration contains the values greater than 1. model 6 predicts the values of A_{fast} smaller than 1 and the only model, which can simulate $A_{fast} > 1$, is model 2. It is model 2 that should also be contained in the resulting model. The simplest appropriate combination of models 2 and 6 is as follows:

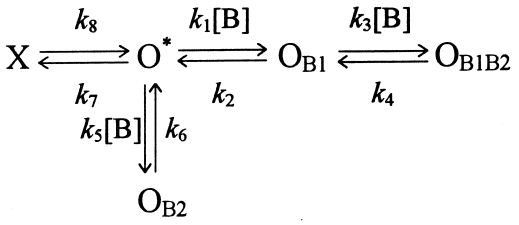

Model 7

Without the state designated as O_{B2}, this model, similarly to model 6, is able to simulate only the decrease in A_{fast} with the blocker concentration. For this reason, the existence of O_{B2} is necessary. The state designated as O_{B2} can be designated on equal terms as O_{B3} but an increase in the number of the blocker binding sites is not necessary here. Thus, model 7 can be interpreted in the following way. The blocker molecule can bind to sites 1 or 2 when the channel is in the open state (O*). The binding of one blocker molecule to the shallow site 2 prevents the other molecule to reach the vacant site 1 located deep in the channel pore. The binding of the blocker directly to site 2 allows the other blocker to bind to site 1.

Table 2
The kinetic constants for 9-AA

Kinetic constant	Value
k_1	2.9×10^7 M^{-1} s^{-1}
k_2	10^3 s^{-1}
k_3	0.74×10^6 M^{-1} s^{-1}
k_4	1.54 s^{-1}
k_5	0.54×10^5 $M^{-1}s^{-1}$
k_6	0.47 s^{-1}
k_7	0.17 s^{-1}
k_8	0.3 s^{-1}

The increase in A_{fast} with 9-AA concentration can be explained in the following way. Let the transitions from O_{B1} to O and from O_{B1B2} to O_{B1} be faster than those from X to O and from O_{B2} to O. Then the amplitude of the fast component is defined as a ratio of the total number of channels in states O_{B1} and O_{B1B2} and in states X, O_{B1}, O_{B2} and O_{B1B2} at the moment of termination of the blocker application. At low blocker concentrations, the occupation of the O_{B2} state is comparable with those of the O_{B1} and O_{B1B2} states. The number of channels in the latter two states with respect to the total number of channels in X, O_{B1}, O_{B2} and O_{B1B2} states is small and, consequently, A_{fast} is also small. After the increasing of the blocker concentration more and more channels accumulate in the double-blocked O_{B1B2} state. The contribution of O_{B1} and O_{B1B2} states increases and A_{fast} rises with it.

The kinetic constants for model 7 can be estimated as follows. The theory predicts (see Appendix A) that the process of the current recovery after termination of the blocker application is described by a sum of four exponents with the following time constants: $\tau_1 = 1/(k_7 - k_8)$; $\tau_2 = 1/k_2$; $\tau_3 = 1/k_4$; $\tau_4 = 1/k_6$. As the value of τ_{fast} at 2.5 μM 9-AA (180 ± 147 ms) did not differ significantly from the switching solution time ($\tau_{OFF} = 137 \pm 71$ ms), it seemed correct to suggest the existence of a very fast component of the channels recovery from the 9-AA block, which was masked by the process of the solution exchange as it was suggested in the cases of TBA and TEA. Therefore, the value of the dissociation constant of the fastest transition, k_2, was adopted as 1000 s^{-1}. The increase in the τ_{fast} value with 9-AA concentration and its attainment of the stationary level (649 ± 147 ms) at 40 μM (Fig. 8B) may be considered as evidence of enhancement and saturation in the occupation of the O_{B1B2} state of the channel. Therefore, the value of the dissociation constant of the rate-limiting fast transition, k_4, was adopted as 1/0.649 s = 1.54 s^{-1}. The slow dissociation constant, k_6, was estimated from the value of the slow time constant, which did not depend on 9-AA concentration (Fig. 8C): $k_6 = 1/\tau_{slow} = 0.47$ s^{-1}. Eq. A12 (see Appendix A) defines the amplitude of the fast component for model

7 as:

$$A_{fast} = \frac{1 + a \cdot [B]}{b + c \cdot [B]} \quad (9)$$

where

$$a = \frac{k_2 \cdot k_3 \cdot (k_2 - k_7 - k_8)}{(k_2 - k_4) \cdot (k_2 - k_8)} \left\{ \frac{k_4 - k_8}{k_4 \cdot (k_4 - k_7 - k_8)} - \frac{k_2 - k_8}{k_2 \cdot (k_2 - k_7 - k_8)} \right\}$$

$$b = \frac{k_2 \cdot k_8 \cdot (k_2 - k_7 - k_8)}{k_1 \cdot (k_7 + k_8) \cdot (k_2 - k_8)} \left\{ \frac{k_1}{k_2} + \frac{k_5}{k_6} \right\}$$

$$c = \frac{k_3 \cdot k_8 \cdot (k_2 - k_7 - k_8)}{k_4 \cdot (k_7 + k_8) \cdot (k_2 - k_8)}$$

The A_{fast} defined by Eq. 9 increases with the blocker concentration when $a \cdot b > c$, decreases when $a \cdot b < c$, and is constant (equal to $1/b$) when $a \cdot b = c$. The fitting of the A_{fast} dependence on 9-AA concentration by Eq. 9 (Fig. 8D) and of the I_B/I_S dependence on 9-AA concentration by Eq. A13 (Fig. 8E) gave only four independent equations for determination of the kinetic constants k_1, k_3, k_5, k_7 and k_8. The solutions of this system of equations were found at different values of k_8, which varied from 0 to 1.5 s^{-1} (at $k_8 > 1.5$ s^{-1} A_{fast} did not increase but decreased with a rise in 9-AA concentration). At $k_8 = 0.3$ s^{-1} the current curves predicted by model 7 (Fig. 8A, second row) looked like those in the experiment. The corresponding values of the kinetic constants for model 7 in this case are presented in Table 2.

4. Discussion

The present study offers a method for determining the simplest kinetic model for the blocker interaction with a ligand-gated channel proceeding from the manifested two-component kinetics. The use of this method supplemented, wherever possible, by other experimental data yields valuable information about the origin of the kinetic components and the information for constructing a physical model of the channel–blocker interaction. It provides the answers to the following questions: How does the blocker interact with the gating machinery of the channel? How many blocker binding sites in the channel, what is the sequence and scheme of their occupation? The criterion of finding the best model is the behavior of the amplitude of the fast component (A_{fast}) as a function of the blocker concentration. Depending on the value and constancy or a decrease in A_{fast} with the blocker concentration, the blocker action can be described by one of the five simplest kinetic models (models 2–6). Models 2–5 predict the blocking kinetics when A_{fast} does not depend on the blocker concentration (Eqs. 4–7). These models differ by the predicted range of A_{fast} value: for model 2 this parameter can be of any value, for model 3 and 4 is greater than 0 but smaller than 1, while for model 5 it is always negative. Model 6 predicts the blocking kinetics when A_{fast} decreases with the blocker concentration (Eq. 8). The examples of the blockers, the action of which can be described by the simplest kinetic models, are provided by the NMDA open channel blockers: TBA, TEA and MRZ.

The value of A_{fast} for TBA did not depend on the blocker concentration and was greater than 1. Therefore, within the framework of the simplest kinetic models the effect of TBA can be described only by model 2. The X state of this model can be the closed or the desensitized or some combination of the closed and the desensitized states of the channel. However, the time constants of the transitions from the closed to the open state of the NMDA channel and reverse are much faster than those defined by the kinetic constants, k_3 and k_4, for model 2 (Table 1). Thus, the smallest value of the kinetic constant for the transition from the open to the closed state (140 s^{-1}) is estimated from the mean open time varying in single NMDA channel experiments from 2.5 to 7 ms [22–24]. Knowing this constant and the open probability of NMDA channels, P_0, it is easy to estimate the kinetic constant of the transition from the closed to the open state. As it has been mentioned above, in the majority of studies the value of P_0 was estimated as being rather great (0.2–0.5). But even if we adopt the smallest value of 0.04 [21], the kinetic constant of the transition from the closed to the open state (6 s^{-1}) will prove to be 3–4-times higher than k_3 and k_4 for TBA. Therefore, the X state in model 2 is more probably the desensitized one or represents a combination of the closed and the desensitized states of the channel. Thus, model 2 shows that the NMDA chan-

nel can close and/or desensitize in the open conducting state, while this channel cannot do it when blocked by TBA. Such asymmetry of model 2 points to the interaction of the blocker with the gating machinery of the NMDA channel. TBA bound to its blocking site prevents the closure of the activation and/or desensitization gates of the NMDA channel. This fact has been established in the experiments where the ASP and TBA coapplication was followed by the transient current increase (the so-called 'hook' current), which exceeded the control current level [8].

With respect to the interaction with the gating machinery of the NMDA channel, it is interesting to compare TBA with another tetraalkylammonium compound, TEA. Its action can be described by models 3 and 4. Model 3 does not contain either closed or desensitized states of the channel and, correspondingly, is symmetric with respect to the ability of the open and the open-blocked state of the channel to close and/or desensitize. The more realistic representation of this model is as follows:

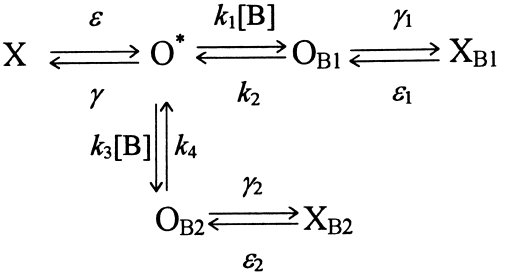

Model 8

where X, X_{B1} and X_{B2} represent the states analogous to those in models 2, 4, 5 and 7. If we suppose for simplicity that TEA does not affect the processes of the channel closure and/or desensitization and, correspondingly, $\gamma = \gamma_1 = \gamma_2$ and $\varepsilon = \varepsilon_1 = \varepsilon_2$, the kinetics predicted by model 8 (Fig. 9A) is qualitatively the same (A_{fast} is within [0,1] interval and does not depend on the blocker concentration) as the kinetics predicted by model 3 (Fig. 5A, second row). The

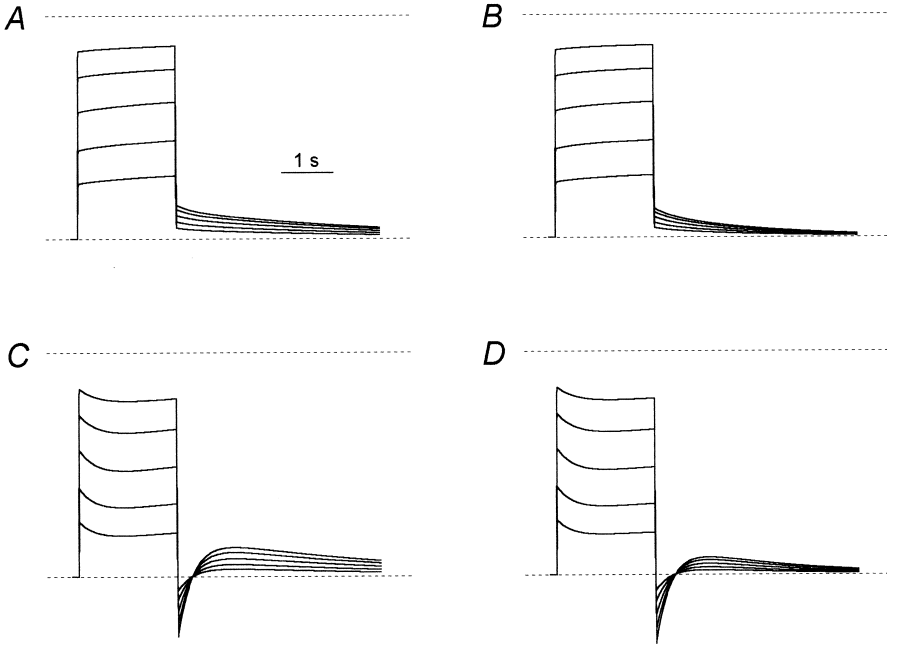

Fig. 9. The kinetics for TEA predicted by model 8. The values of the kinetic constants, k_1, k_2, k_3, and k_4, are the same as in model 3 (see Table 1). The kinetic constants for the transitions O–X, O_{B1}–X_{B1}, and O_{B2}–X_{B2} are the same as for the transition O–X in model 2 for TBA: $\gamma = \gamma_1 = \gamma_2 = 1.52\ s^{-1}$ and $\varepsilon = \varepsilon_1 = \varepsilon_2 = 1.77\ s^{-1}$. TEA concentrations are: 0.625, 1.25, 2.5, 5 and 10 mM. The curves presented are the modeling currents predicted by (A) model 8; $A_{fast} = 0.84$ and does not depend on the blocker concentration; (B) model 8 without the X_{B2} state; $A_{fast} = 0.86$ and does not depend on the blocker concentration; (C) model 8 without the X_{B1} state; (D) model 8 without the X_{B1} and X_{B2} states. In C and D the overshoot of the modeling current ($A_{fast} > 1$) is observed.

removal of the X_{B2} state next to the slow blocked state, O_{B2}, from model 8 does not change this kinetics significantly (Fig. 9B). However, removal of the X_{B1} state next to the fast blocked state, O_{B1}, from model 8 leads to the appearance of the current overshoot ($A_{fast} > 1$), which resembles that observed in the kinetics of TBA (Fig. 9C,D). Therefore, TEA binding to the channel in the fast blocked state, O_{B1}, does not prevent the closure of the activation and/or desensitization gate. Whether this is true for TEA binding to the channel in the slow blocked state, O_{B2}, remains unclear because the O_{B2}–X_{B2} transition is faster than the transition from O_{B2} to O.

The X_B state in model 4 can be interpreted as: (1) the second open blocked (O_{B2}) and (2) closed blocked (C_B) or desensitized blocked (D_B), or a combination of the closed and the desensitized blocked states of the channel. In the first case, the transition from O_{B1} to O_{B2} means a 'jump' of the blocker from one blocking site to another. The succession of binding of the blocker molecule to the sites is strict: at first site 1 becomes occupied and then site 2 follows it. In this case, models 3 and 4 can represent the parts of a more complex model with the transitions O_{B1}–O_{B2}, O–O_{B1} and O–O_{B2} (a combination of models 3 and 4). Such a model describes the situation when the only blocker molecule can bind to any of the two blocking sites in the channel in any succession and can 'jump' from one blocking site to another. Thus, in the first case model 4 is symmetric with respect to the ability of the open and the open-blocked state of the channel to close and/or desensitize. The more realistic representation of this model is as follows:

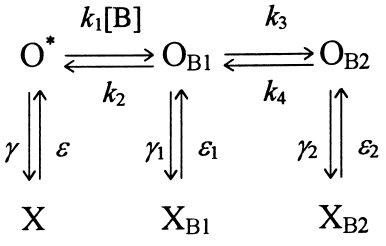

Model 9

As in the case of model 8, the kinetics predicted by model 9 is qualitatively the same as the kinetics predicted by model 3 (Fig. 5A, second row). The removal of X_{B2} state does not significantly change the recovery kinetics, while the removal of X_{B1} state leads to the appearance of the current overshoot ($A_{fast} > 1$), which resembles that observed in the kinetics of TBA. Therefore, TEA binding to the channel in state O_{B1} does not prevent the closure of the activation and/or desensitization gate of the channel. Whether this is true for TEA binding to the channel in state O_{B2} remains unclear because the O_{B2}–X_{B2} transition is faster than the O_{B2}–O_{B1} transition.

In the second case, the existence of the closed or desensitized (or their combination) states of the blocked channel and their absence in the non-blocked channel may imply: (a) the ability of the blocker to increase the number of closed blocked and/or desensitized blocked states when the more realistic representation of model 4 is as follows:

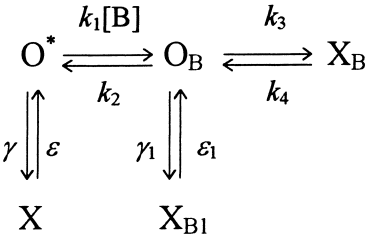

Model 10

and (b) the channel closes and/or desensitizes more readily with the blocker inside (the state X_{B1} is absent in model 10 but the O_B–X_B equilibrium is shifted to X_B with respect to model 4). Both (a) (Fig. 10A) and (b) (Fig. 10B) possibilities demonstrate the kinetics, which are qualitatively similar (A_{fast} is within the [0,1] interval and does not depend on the blocker concentration) to that predicted by model 4 (Fig. 5A, second row), but quite different from that which is predicted by model 4 with addition of only the X state similar to model 2 for TBA (or by model 10 without the X_{B1} state) (Fig. 10C).

Thus, all the simplest models (3 and 4) describing the mechanism of TEA action predict that this blocker does not prevent the closure of the activation and/or desensitization gates of the NMDA channel when bound to at least one site and even possibly promotes this process.

The difference in the interaction of tetraalkylammonium compounds with the gating machinery of

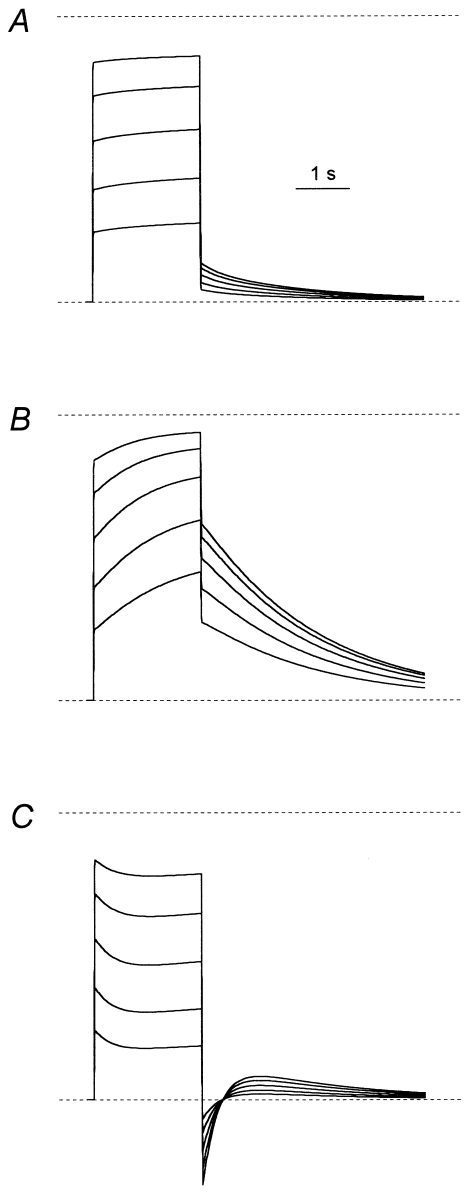

Fig. 10. The kinetics predicted by model 10 for TEA. The values of the kinetic constants, k_1, k_2 and k_4, are the same as in model 4 (see Table 1). The kinetic constants for the transitions O–X and O_B–X_{B1} are the same as for the transition O–X in model 2 for TBA: $\gamma = \gamma_1 = 1.52\ s^{-1}$ and $\varepsilon = \varepsilon_1 = 1.77\ s^{-1}$. TEA concentrations are 0.625, 1.25, 2.5, 5 and 10 mM. The curves presented are the modeling currents predicted by (A) model 10; the value of $k_3 = 118\ M^{-1}s^{-1}$ is the same as in model 4; $A_{fast} = 0.86$ and does not depend on the blocker concentration; (B) model 10 without the X_{B1} state; the value of $k_3 = 1180\ M^{-1}s^{-1}$ is ten times higher than that in model 4; $A_{fast} = 0.33$ and does not depend on the blocker concentration; (C) model 10 without the X_{B1} state; the value of $k_3 = 118\ M^{-1}s^{-1}$ is the same as in model 4. In C the overshoot of the modeling current ($A_{fast} > 1$) is observed.

the NMDA channel can be explained by different size of the blocking molecules [25]. Thus, the larger blocker, TBA, prevents the closure of activation and/or desensitization gates, while the smaller one, TEA, which enters deep into the channel pore allows the gates to close after it.

The value of A_{fast} decreased with MRZ concentration. The only simplest model describing qualitatively such A_{fast} behavior is model 6. This model suggested the existence of two non-overlapping blocking sites of MRZ in the open NMDA channel. These two sites can be occupied simultaneously by different blocker molecules and the succession is strict: site 1 is occupied at first, and site 2 is occupied secondly. In reality, the situation may be more complex. It is correct to suppose that the blocker can reach site 1 not only directly from the external solution but also by way of sequential 'jumps' from the external solution to site 2 and then to site 1 [4]. Thus, the transition O^*–O_{B1} of model 6 can imply two sequential transitions: O^*–O_{B2} and O_{B2}–O_{B1}. Contrary to TBA and TEA, the kinetics of the MRZ-induced blockade is much slower than the kinetics of NMDA channel closure and desensitization. Therefore, the more realistic version of model 6:

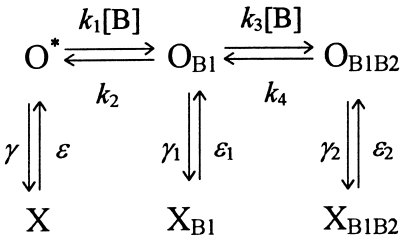

Model 11

demonstrates practically the same recovery kinetics as model 6 (Fig. 7A, second row) in all possible cases when: (1) X_{B1}, or (2) X_{B1B2}, or (3) X_{B1} and X_{B1B2} states are removed, or (4) all states of model 11 are present. The fact is that the method used in the present study cannot answer the question 'Does the blocker prevent the closure of the activation and/or desensitization gate of NMDA channel?' concerning the blockers with such slow kinetics as that of MRZ because this method is applicable only for fast blockers [8]. However, other experiments do provide an answer to this question. Thus, the ability of another

aminoadamantane derivative, memantine, differing from MRZ by two methyl groups and hydrogen instead of one propyl and two hydrogen attached to three equivalent sites of 1-adamantanamine, to produce the trapping block of NMDA channels has been reported previously [5,26]. (1) The existence of two components in the kinetics of agonist-induced channels recovery after MEM-induced open-channel block and subsequent washout of the cell in an agonist-free solution [3], and (2) the fact that two similar components in the recovery kinetics of MEM in the continuous presence of agonist were explained by simultaneous occupation by MEM of two different blocking sites in the NMDA channel [4] strongly suggest that both MEM blocking sites are located below the activation gate and two MEM molecules bound to them can be closed within the NMDA channel. The data obtained in our laboratory (unpublished observation) indicate that in all probability this is also true for MRZ.

The only simplest model which remained without an example of a blocker is model 5. This model predicts the blocker association not with the open but mainly with the closed and/or desensitized states of the channel. In my opinion, up to now nobody has studied the NMDA channel blocker with the kinetics predicted by model 5 ($A_{fast} < 0$ and does not depend on the blocker concentration). Probably, such a blocker will be found in future.

In the case when the blocker-induced kinetics cannot be described by any of the simplest models the method of the simplest models combination can be used. Thus, not every simplest model describes the increase in A_{fast} with the blocker concentration. Such behavior of A_{fast} can be obtained by combination of model 6, the only simplest model predicting a change in A_{fast} with the blocker concentration, with one or several from models 2–5. 9-AA is an example of an NMDA open-channel blocker, the amplitude of the fast component for which increased with concentration.

As A_{fast} was greater than unity at high 9-AA concentrations, the simplest model simulating 9-AA kinetics (except for model 6) should contain model 2. The resulting model 8 predicts the existence of at least two non-overlapping 9-AA blocking sites, which can be simultaneously occupied by two different blocker molecules in two different successions. model 7 is asymmetric with respect to the ability of the channel to close and/or desensitize in the blocked and the non-blocked states. It predicts that 9-AA bound to the channel prevents the closure of the

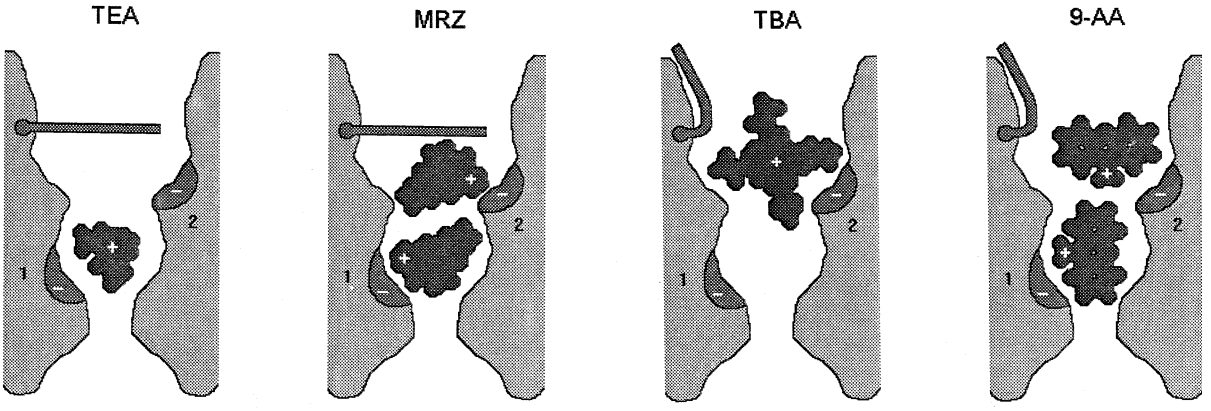

Fig. 11. Possible interpretation of the NMDA open-channel block by organic cations. The smallest cation, TEA, can bind either to the deep blocking site 1 or the shallow blocking site 2 and does not prevent the closure of the gate. Strong electrical repulsion of two TEA molecules prevents their simultaneous occupation of the sites. On the contrary, two molecules of MRZ being electrical dipoles can bind to the two blocking sites simultaneously and do not prevent the closure of the gate. Due to its large size, the TBA molecule can bind only to the shallow site 2 and thus prevents the closure of the gate. When oriented along the channel pore, the 9-AA molecule can quickly reach the deep site 1 (right from the external solution or by way of sequential 'jumps' from the external solution to site 2 and then to site 1 as is in the case with MRZ) and allow another 9-AA molecule to bind to site 2 in the orientation across the channel pore. When site 1 is vacant and the binding of the 9-AA molecule to the shallow site 2 proceeds in orientation across the channel pore, the channel constriction between sites 1 and 2 prevents the 9-AA molecule binding to site 2 to 'jump' to site 1.

activation and/or desensitization gates. The ability of 9-AA to prevent the closure of the NMDA channel was reported previously [9,19,8].

Previous studies on the open-channel structure allow to represent the NMDA channel as a pore with large extracellular and small cytoplasmic mouths. The narrow part of the pore (selectivity filter) is short and has a cross-sectional area of 22–26 $Å^2$ [27,28]. Based on the results of kinetic analysis presented for TBA, TEA, MRZ and 9-AA, the simplest physical models of the open NMDA channel interaction with organic cations can be suggested (Fig. 11).

The simplest kinetic models describing the effects of NMDA open-channel blockers with the constants collected in Tables 1 and 2 have significance in principle but do not pretend to describe completely all the possible states and substates of the NMDA channel. Simplification of the models presented above can be seen in the following facts. The value of k_2 (10^3 s^{-1}) for TBA, TEA and 9-AA was chosen arbitrarily. This value can be much higher. An increase in the value of k_2 may cause a considerable change in the value of k_1, although other kinetic constants will not vary significantly. The values of k_3 and k_7 as well as the values of k_4 and k_8 in model 2 for TBA and in model 7 for 9-AA, respectively (see Tables 1 and 2), were different, although the physical meaning of these constants was the same. The concentration dependence of the fraction of the stationary block by MRZ predicted by model 6 was steeper than that obtained in the experiment (see Fig. 7E). Depending on the problem, each of the simplest models can be complicated by addition of multiple closed, desensitized and open states of the channel. The existence of different populations of the channels can also be taken into account. However, all these changes will not concern such questions of principle as the minimal number of simultaneously occupied blocking sites in the channel and the minimal number of the ways, by which the blocker can reach these sites [4] and the ability of the blocker being bound to the channel to prevent or not prevent the closure of the activation and/or the desensitization gates.

Acknowledgements

The author thanks B.I. Khodorov and S.G. Koshelev for critical discussions, and R.L. Birnova for help in preparation of the manuscript. I am also very grateful to the colleagues at MERZ and Co. for the generous supply of 1-amino-3-propyl-adamantane (MRZ 2/178). This work has been supported by the RFBR (N 96 04 49228), and ISSEP (N a98-2018).

Appendix A

Let $X(t)$ be the vector of probabilities of the channel occupying each of all possible states at the time, t. The behavior of $X(t)$ is defined by the linear system of differential equations:

$$\frac{dX(t)}{dt}\mathbf{A}X(t) \tag{A1}$$

where **A** is the matrix of transitions between the states of the channel. To solve system A1, it is necessary to find all the eigenvalues of **A** by solving the following equation:

$$|\mathbf{A}-\lambda\mathbf{E}| = 0 \tag{A2}$$

where λ is variable and **E** is the matrix with the diagonal elements equal to 1 and the nondiagonal elements equal to 0. In the case of the simplest models presented in this study, Eq. A2 has no multiple roots and the solution of Eq. A1 can be written in the following form:

$$X(t) = \sum_{i=1}^{n} C_i v_i e^{\lambda i t} \tag{A3}$$

where C_i is the ith constant; v_i is the ith eigenvector of **A** corresponding to the ith eigenvalue, λ_i; n is the number of states. The constants C_i ($i = 1,...,n$) can be estimated from the probabilities of the channel to be in all possible states at equilibrium by posing $t = 0$ in Eq. A3. Each of models 2–6 has its own transition matrix with elements representing the sums of the kinetic constants multiplied, where necessary, by the blocker concentration. The number of states is equal to 3, and the solution of Eq. A2 gives three values of λ: $\lambda_1 = 0$ and $\lambda_2, \lambda_3 \neq 0$. Let λ_2 correspond to the fast and λ_3 to the slow component of the kinetics. When [B] = 0, there is a case of the channels recovery after the block. The fast and the slow time

constants of the channels recovery, τ_{fast} and τ_{slow}, respectively, are given by the following equations:

$$\lambda_2(k_1,\ k_2,\ k_3,\ k_4) = -1/\tau_{fast} \quad (A4)$$

$$\lambda_3(k_1,\ k_2,\ k_3,\ k_4) = -1/\tau_{slow} \quad (A5)$$

where $\lambda_2(k_1,\ k_2,\ k_3,\ k_4)$ and $\lambda_3(k_1,\ k_2,\ k_3,\ k_4)$ are defined from the solution of Eq. A2 relative to λ_2 and λ_3.

To determine the probabilities of the channel to be in all possible states at equilibrium ($t=0$), the right part of Eq. A1 should be taken as being equal to zero. Thus, we obtain a system of n linear equations:

$$\mathbf{A}\cdot\mathrm{X}(0) = 0 \quad (A6)$$

with n variables: $x_1(0),...,x_n(0)$. As the rank of $\mathbf{A}$ is equal to $n-1$, only $n-1$ equations are independent. Adding the equation of the sum of probabilities of the channel occupying each of all possible states:

$$x_1(0) + x_2(0) + ... + x_n(0) = 1 \quad (A7)$$

we obtain a system of n equations with n variables which allows to determine the probabilities of the channel occupying each of all possible states at equilibrium in terms of kinetic constants. The fraction of non-blocked channels at equilibrium at the [B] blocker concentration is defined via the probabilities of the open (jth) state occupancy in the absence, $[O]_{[B]=0} = x_j(0)_{[B]=0}$, and the presence, $[O]_{[B]\neq 0} = x_j(0)_{[B]\neq 0}$, of the blocker, respectively:

$$d = [O]_{[B]\neq 0}/[O]_{[B]=0} \quad (A8)$$

The calculation of d for models 2–5 leads to the following equation:

$$d = \frac{1}{1 + K\cdot[B]} \quad (A9)$$

where K is equal to $k_1\cdot k_4/k_2/(k_3+k_4)$ for model 2, $k_1/k_2+k_3/k_4$ for model 3, $k_1\cdot(1+k_3/k_4)/k_2$ for model 4 and $k_1\cdot k_3/k_4/(k_1+k_2)$ for model 5. Only the denominator of the equation for model 6 contains the item with [B] rose to the second power:

$$d = \frac{1}{1 + (k_1/k_2)\cdot[B] + (k_1\cdot k_3/k_2/k_4)\cdot[B]^2} \quad (A10)$$

The amplitude of the fast component, A_{fast}, for models 2–6 is determined from Eq. A3 for the probability of the open (jth) state occupancy:

$$A_{fast}(k_1,\ k_2,\ k_3,\ k_4, [B]) = \frac{C_2\cdot\nu_{2j}}{C_2\cdot\nu_{2j} + C_3\cdot\nu_{3j}} \quad (A11)$$

The substitution of the mean experimental values of the fast and slow time constants into Eq. A4 and Eq. A5, the estimation of the parameters of Eq. A9 or Eq. A10 due to the fitting of the experimental I_B/I_S dependence on the blocker concentration and the parameters of Eq. A11 due to the fitting of the experimental A_{fast} dependence on the blocker concentration give a system of equations which allows to determine all the kinetic constants: k_1, k_2, k_3 and k_4. The values of the kinetic constants for TBA, TEA and MRZ are presented in Table 1.

Model 7 contains five states of the channel. The eigenvalues for the recovery process defined from Eq. A2 are the following: $\lambda_1 = 0$; $\lambda_2 = -k_7 - k_8$; $\lambda_3 = -k_2$; $\lambda_4 = -k_4$; $\lambda_5 = -k_6$. If the amplitude of the fast component is defined as the ratio of changes in the total number of channels in O_{B1} and O_{B1B2} states and in the total number of channels in C, O_{B1}, O_{B2} and O_{B1B2} states induced by a removal of the blocker, then A_{fast} will be defined from Eq. A3 as follows:

$$A_{fast} = \frac{C_3\cdot\nu_{3j} + C_4\cdot\nu_{4j}}{C_2\cdot\nu_{2j} + C_3\cdot\nu_{3j} + C_4\cdot\nu_{4j} + C_5\cdot\nu_{5j}} \quad (A12)$$

Eq. A8 for the fraction of non-blocked channels at equilibrium for model 7 is defined by the following way:

$$d = \frac{1}{1 + a\cdot[B] + b\cdot[B]^2} \quad (A13)$$

where

$$a = \frac{k_8\cdot(k_1/k_2 + k_5/k_6)}{k_7 + k_8};\ b = \frac{k_1\cdot k_3\cdot k_8}{k_2\cdot k_4\cdot(k_7 + k_8)}$$

References

[1] T. Frankiewicz, B. Potier, Z.I. Bashir, G.L. Collingridge, C.G. Parsons, Effects of memantine and MK-801 on NMDA-induced currents in cultured neurones and on synaptic transmission and LTP in area CA1 of rat hippocampal slices, Br. J. Pharmacol. 117 (1996) 689–697.

[2] I. Bresink, T.A. Benke, V.J. Collett, A.J. Seal, C.G. Parsons,

J.M. Henley, G.L. Collingridge, Effects of memantine on recombinant rat NMDA receptors expressed in HEK 293 cells, Br. J. Pharmacol. 119 (1996) 195–204.
[3] T.A. Blanpied, F. Boeckman, E. Aizenman, J.W. Johnson, Trapping channel block of NMDA-activated responses by amantadine and memantine, J. Neurophysiol. 77 (1997) 309–323.
[4] A. Sobolevsky, S. Koshelev, Two blocking sites of amino-adamantane derivatives in open *N*-methyl-D-aspartate channels, Biophys. J. 74 (1998) 1305–1319.
[5] J.W. Johnson, S.M. Antonov, T.S. Blanpied, Y. Li-Smerin, Channel block of NMDA receptor, in: H.V. Wheal (Ed.), Excitatory Amino Acids and Synaptic Transmission, Academic Press, London, 1995, pp. 99–113.
[6] S.M. Antonov, J.W. Johnson, N.Y. Lukomskaya, N.N. Potapyeva, V.E. Gmiro, L.G. Magazanik, Novel adamantane derivatives act as blockers of open ligand-gated channels and as anticonvulsants, Mol. Pharmacol. 47 (1995) 558–567.
[7] S.G. Koshelev, B.I. Khodorov, Tetraethylammonium and tetrabutylammonium as tools to study NMDA channels of the neuronal membrane, Biologicheskie Membrany 9 (1992) 1365–1369.
[8] S.G. Koshelev, B.I. Khodorov, Blockade of open NMDA channel by tetrabutylammonium, 9-aminoacridine and tacrine prevents channels closing and desensitization, Membr. Cell Biol. 9 (1995) 93–109.
[9] A.C.S. Costa, E.X. Albuquerque, Dynamics of the actions of tetrahydro-9-aminoacridine and 9-aminoacridine on glutamatergic currents: Concentration-jump studies in cultured rat hippocampal neurons, J. Pharmacol. Exp. Ther. 268 (1994) 503–514.
[10] W. Danysz, C.G. Parsons, I. Bresink, G. Quack, Glutamate in CNS disorders, DN and P 8 (1995) 261–277.
[11] V.S. Vorobjev, Vibrodissociation of sliced mammalian nervous tissue, J. Neurosci. Methods 38 (1991) 145–150.
[12] M. Benveniste, J.-M. Mienville, E. Sernagor, M.L. Mayer, Concentration-jump experiments with NMDA antagonists in mouse cultured hippocampal neurons, J. Neurophysiol. 63 (1990) 1373–1384.
[13] M. Benveniste, J. Clements, L. Vyklicky, M.L. Mayer, A kinetic analysis of the modulation of *N*-methyl-D-aspartic acid receptors by glycine in mouse cultured hippocampal neurones, J. Physiol. 428 (1990) 333–357.
[14] P. Ascher, L. Nowak, The role of divalent cations in the *N*-methyl-D-aspartate responses of mouse central neurones in culture, J. Physiol. 399 (1988) 247–266.
[15] J.M. Wright, P.A. Kline, L.M. Nowak, Multiple effects of tetraethylammonium on *N*-methyl-D-aspartate receptor-channels in mouse brain neurons in cell culture, J. Physiol. 439 (1991) 579–604.
[16] F. Lin, C.F. Stevens, Both open and closed NMDA receptor channels desensitize, J. Neurosci. 14 (1994) 2153–2160.
[17] C.E. Jahr, High probability opening of NMDA receptor channels by L-glutamate, Science 255 (1992) 470–472.
[18] R.A.J. Lester, G. Tong, C.E. Jahr, Interactions between the glycine and glutamate binding sites of the NMDA receptor, J. Neurosci. 13 (1993) 1088–1096.
[19] M. Benveniste, M.L. Mayer, Trapping of glutamate and glycine during open channel block of rat hippocampal neuron NMDA receptors by 9-aminoacridine, J. Physiol. 483 (1995) 367–384.
[20] D. Colquhoun, A.G. Hawkes, Desensitization of *N*-methyl-D-aspartate receptors: a problem of interpretation, Proc. Natl. Acad. Sci. U.S.A. 92 (1995) 10327–10329.
[21] C. Rosenmund, A. Feltz, G.L. Westbrook, Synaptic NMDA receptor channels have a low open probability, J. Neurosci. 15 (1995) 2788–2795.
[22] P. Ascher, P. Bregestovski, L. Nowak, *N*-Methyl-D-aspartate-activated channels of mouse central neurones in magnesium-free solutions, J. Physiol. 399 (1988) 207–226.
[23] S.G. Cull-Candy, M.M. Usowich, On the multiple-conductance single channels activated by excitatory amino acids in large cerebellar neurones of the rat, J. Physiol. 415 (1989) 555–582.
[24] C.E. Jahr, C.F. Stevens, A quantitative description of NMDA receptor-channel kinetic behavior, J. Neurosci. 10 (1990) 1830–1837.
[25] S. Koshelev, B. Khodorov, Probing of NMDA receptor channels by organic cations. Location of activation and inactivation gates, in: J. Lerma, P.H. Seeburg (Orgs.), Workshop on Molecular Mechanisms of Synaptic Function, Madrid, 1994, p. 64.
[26] H.-S.V. Chen, S.A. Lipton, Mechanism of memantine block of NMDA-activated channels in rat retinal ganglion cells: uncompetitive antagonism, J. Physiol. 499 (1997) 27–46.
[27] M.M. Zarei, J.A. Dani, Structural basis for explaining open-channel blockade of the NMDA receptor, J. Neurosci. 15 (1995) 1446–1454.
[28] A. Villarroel, N. Burnashev, B. Sakmann, Dimensions of the narrow portion of a recombinant NMDA receptor channel, Biophys. J. 68 (1995) 866–875.